

Supporting Information

A Hollow MOF-derived Capsular $V_xO_3@CN$ Cathode with High Capacity and Ultralong Lifespan for Aqueous Zinc Ion Battery

Hongwen Liu,^{acc†} Jialong Jiang,^{a†} Yong-Sheng Wei,^c Runhao Zhang,^a Jiachen Guo,^a Jingwei Liu,^a Peng Cheng,^{ab} Qiang Xu^{*cd} and Wei Shi^{*a}

a. State Key Laboratory of Advanced Chemical Power Sources, Frontiers Science Center for New Organic Matter, and Key Laboratory of Advanced Energy Materials, Chemistry (MOE), College of Chemistry, Nankai University, Tianjin 300071, China. E-mail: shiwei@nankai.edu.cn

b. Haihe Laboratory of Sustainable Chemical Transformations, Tianjin 300192, China

c. AIST-Kyoto University Chemical Energy Materials Open Innovation Laboratory (ChEM-OIL) National Institute of Advanced Industrial Science and Technology (AIST) Yoshida, Sakyo-ku, Kyoto 606-8501, Japan. E-mail: xu.qiang@icems.kyoto-u.ac.jp

d. Shenzhen Key Laboratory of Micro/Nano-Porous Functional Materials (SKLPM), SUSTech-Kyoto University Advanced Energy Materials Joint Innovation Laboratory (SKAEM-JIL), and Department of Chemistry, Southern University of Science and Technology (SUSTech), Shenzhen 518055, China. E-mail: xuq@sustech.edu.cn

e. Shenzhen BYD Lithium Battery Co., Ltd. Kengzi Branch, Shenzhen, China.

[†] These authors contributed equally to this work.

Contents	
Sample synthesis	3-4
Characterizations	5-6
Computational Details	7
Figure S1	SEM images of V-NH ₂ -MIL88B 8
Figure S2	FT-IR spectra of tpy, V-NH ₂ -MIL88B and capsular MOF 9
Figure S3	SEM images of capsular MOF 10
Figure S4	TEM image and the EDS mapping images of capsular MOF 11
Figure S5	TGA curve of capsular MOF 12
Figure S6	DFT calculation of the structural transformation mechanism between V-NH ₂ -MIL88B and capsular MOF 13
Figure S7	Time-dependent PXRD patterns for capsular MOF 14
Figure S8	SEM images of time-dependent intermediates in the synthetic process of capsular MOF 15
Figure S9	PXRD pattern of C-MOF-600. 16
Figure S10	PXRD pattern of C-MOF-800. 17
Figure S11	Raman spectra of V _x O ₃ @CN 18
Figure S12	SEM images of V _x O ₃ @CN 19
Figure S13	XPS spectra of V _x O ₃ @CN 20
Figure S14	PXRD patterns of V _x O ₃ @CN and V _x O ₃ @CN-E 21
Figure S15	Contact angle images of V ₂ O ₃ and V _x O ₃ @CN. 22
Figure S16	Cyclability of C-MOF-600 and C-MOF-800 electrode at 0.5 A g ⁻¹ 23
Figure S17	Calculated spin-polarized total density of states (DOS) plots 24
Figure S18	Charge density difference plots of V ₂ O ₃ -Zn, defective V ₂ O ₃ -Zn 25
Figure S19	Raman spectra of V _x O ₃ @CN electrode 26
Figure S20	Post-cycle PXRD of V _x O ₃ @CN electrode 27
Table S1	Vanadium-based cathode for rechargeable aqueous zinc battery. 28
Table S2	Defect-engineered cathode materials for rechargeable aqueous zinc battery 29
References	30-33

Sample synthesis:

Preparation of Cathodes and Electrolytes: All raw materials were obtained commercially and utilized directly.

The preparation of 2,4,6-tri(pyridin-4-yl)pyridine (tpy)^[1]: 1-(pyridine-4-yl) ethane (6.0 g, 50 mmol) and isonicotinaldehyde (2.7 g, 25 mmol) were added to the ethanol (200 mL) solution of potassium hydroxide (3.1 g, 55 mmol) and 36% ammonium hydroxide (100 mL) were successively added to the above solution. The solution was stirred at room temperature for 24 hours. The mixture was centrifuged and washed with water and ethanol. The obtained solid was dried in a vacuum at 100 °C for 12 hours to obtain a gray-white product (5.6 g, yield ~ 70%). ¹H Nuclear magnetic resonance spectra (400 MHz, CDCl₃): δ 8.88–8.79 (m, 6H), 8.15–8.01 (m, 6H), 7.71–7.62 (m, 2H).

Synthesis of V-NH₂-MIL88B: the mixture of vanadium trichloride (III) (VCl₃, 1.57g, 10.0 mmol) and 2-aminoterephthalic acid (1.81 g, 10.0 mmol) were dissolved in anhydrous ethanol (50 mL) and sonicated for 30 minutes. Subsequently, 10 mL hydrochloric acid aqueous solution (2 M) is added to the solution dropwise under stirring. The obtained solution was sonicated for 15 minutes, then moved to a 100 mL autoclave and heated at 120 °C for 48 hours. After that, the green solid was collected by centrifugation and washed with anhydrous ethanol until the supernatant was colorless. The obtained solid was dried in a vacuum at 120 °C for 12 hours, and a green product (1.3 g, yield ~ 75%) was obtained. Anal. Calc. for [V₃(μ₃-O)(bdc-NH₂)₃(H₂O)₃]: C, 38.37; H, 1.61; N, 5.59. Found: C, 38.51; H, 1.71; N, 5.43.

Synthesis of capsular MOF: the mixture of V-NH₂-MIL88B (200 mg) and 2,4,6-tri(pyridin-4-yl)pyridine (tpy, 100 mg) with 10 mL DMF was added to a 25 mL autoclave, which was sealed and heated at 190 °C for 12 hours. After cooling, the solid was centrifuged and washed with DMF and methanol until the supernatant was colorless. The light green solid powder was isolated by filtration. After vacuum drying of the sample at 100 °C for 4 hours, the capsular MOF as a green powder (200 mg) was obtained. Anal. Calc. for [V₃(μ₃-O)(bdc-NH₂)₃(tpy)] : C, 52.41; H, 2.00; N, 9.73. Found: C, 52.51; H, 1.71; N, 9.43.

Preparation of V_xO₃@CN: 500 mg capsular MOF was calcined in Ar atmosphere at 700 °C for 2 hours to obtain V_xO₃@CN (250 mg). For comparison, the capsular MOF was calcined in Ar atmosphere at 600 °C and 800 °C for 2 hours, and the products were named C-MOF-600 and C-MOF-800, respectively.

Preparation of cathode and assembly of battery: V_xO₃@CN, C-MOF-600, and C-MOF-800 were used as cathodes, respectively. Slurries were prepared by mixing cathodes, Ketjen black and polyvinylidene fluoride (PVDF) with a weight ratio of 8:1:1 in N-methyl-2-pyrrolidone (NMP). The paste was coated on the Ti foil current collector and dried in a vacuum at 80 °C for 12 hours. Then the slices were cut to assemble the CR2032 coin batteries. CR2032 batteries were assembled in air, using zinc foil as counter electrode, fiberglass filter paper as separator, and 3M zinc trifluoromethane sulfonate Zn(CF₃SO₃)₂ aqueous solution as electrolyte.

Preparation of electrolyte: 3 M electrolyte was prepared by dissolving Zn(CF₃SO₃)₂ (10.91 g) in H₂O (10 mL).

Characterizations:

Material test: the PXRD patterns were collected on a Rigaku Smartlab SE powder X-ray diffractometer equipped with Cu-K α source ($\lambda = 1.546 \text{ \AA}$). N₂ adsorption/desorption isotherms were measured at 77 K with an automatic volumetric adsorption equipment (Micromeritics ASAP 2020 Plus HD88) after dehydration of the samples at 100 °C under vacuum for 12 h. Elemental analysis was performed using a Vario EL cube CHN analyzer. TGA curves were measured on a METTER TOLEDO TGA 2 analyzer. FESEM images and EDS mapping were performed using HITACHI S5000 and JEOL JSMIT100 microscopes at an accelerating voltage of 20 kV. The Raman spectra were measured by a Renishawin Via Raman microscope spectrometer. TEM images were taken with a JEOL JEM-2299 FS. The measurement of XPS was carried out on a KRATOS ULTRA2 instrument.

Electrochemical Measurements: All the electrochemical properties of the battery were evaluated using CR2032 coin cell with Zn foil anode, V_xO₃@CN cathode, glass fiber separator, and 3 M Zn(CF₃SO₃)₂ electrolyte. Electrochemical tests were performed in the potential range of 0.3–1.6 V using LAND CT2001A charge-discharge units at 25 °C. EIS tests were carried out on a CHI660D electrochemical workstation with a frequency range of 100 kHz to 1Hz. A CHI660D electrochemical workstation was used to perform cyclic voltammetry (CV) analysis. The relationship between the current (i) and scan rate (ν) in the cyclic voltammograms (CV) follows the following empirical formula.

$$i = a\nu^b \quad (1)$$

where a and b are adjustable parameters. This formula can also be expressed as:

$$\log(i) = b \log(v) + \log(a) \quad (2)$$

The b value represents the slope of $\log(i)$ versus $\log(v)$ plot. In general, when the b value is 0.5, it belongs to the diffusion control process; when the b value is equal to 1, it belongs to the surface adsorption (such as capacitance or pseudo-capacitance behavior) control process.^[2]

Quasi-thermodynamic equilibrium potential profiles of the cell were acquired from the galvanostatic intermittent titration technique (GITT) conducted at a 0.05 A g^{-1} for 10 min followed by 30-min open circuit voltage. Diffusion coefficients of ions (D_{GITT}) were calculated from the GITT data according to the following equation by assuming the active material consists of spherical particles with a radius R_s :^[3]

$$D_{\text{GITT}} = \frac{4}{\pi\tau} \left(\frac{R_s}{3}\right)^2 \left(\frac{\Delta E_s}{\Delta E_t}\right)^2 \quad (3)$$

where τ represents the time duration of the current pulse, ΔE_s is the change in the steady-state voltage at the end of two sequential open circuit relaxation periods, ΔE_t is the total change in the cell voltage.

Computational Details:

The calculations were carried out using density functional theory with the PBE form of generalized gradient approximation functional (GGA).^[4] The Vienna ab-initio simulation package (VASP)^[5-8] was employed. For V, the Hubbard U correction is considered for 3d orbital with an effective U value of 1.7 eV.^[9] The plane wave energy cutoff was set as 400 eV. The Fermi scheme was employed for electron occupancy with an energy smearing of 0.1 eV. The first Brillouin zone was sampled in the Monkhorst–Pack grid.^[10] The 3×3×1 k-point mesh for the surface calculation. The energy (converged to 1.0×10^{-6} eV/atom) and force (converged to 0.01 eV/Å) were set as the convergence criterion for geometry optimization. The spin polarization was considered in all calculations. k-point sampling: $4 \times 4 \times 1$ Monkhorst-Pack grid; Energy convergence criterion: $\leq 1 \times 10^{-5}$ eV/atom; Force convergence threshold: ≤ 0.01 eV/Å.

The transition state (TS) structures and the reaction pathways were located using the climbing image nudged elastic band (CI-NEB) method.^[11] The minimum energy pathway was optimized using the force-based conjugate-gradient method until the maximum force was less than 0.03 eV/Å.

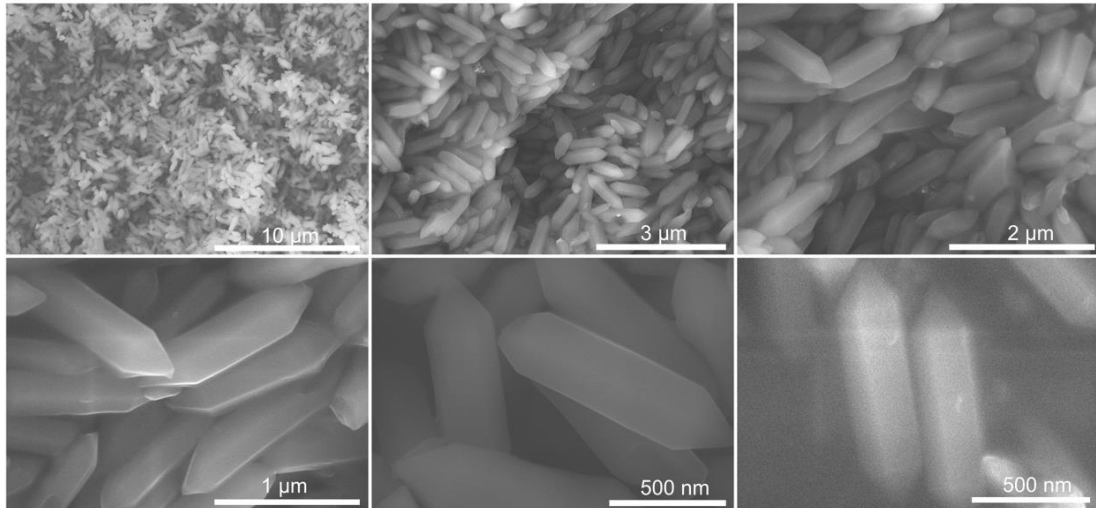


Figure S1. SEM images of V-NH₂-MIL88B.

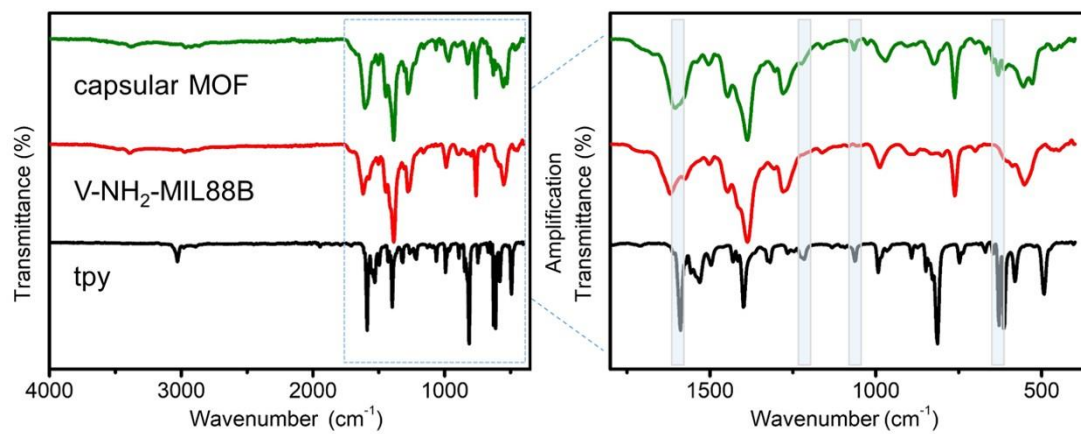


Figure S2. FT-IR spectra of tpy, V-NH₂-MIL88B and capsular MOF.

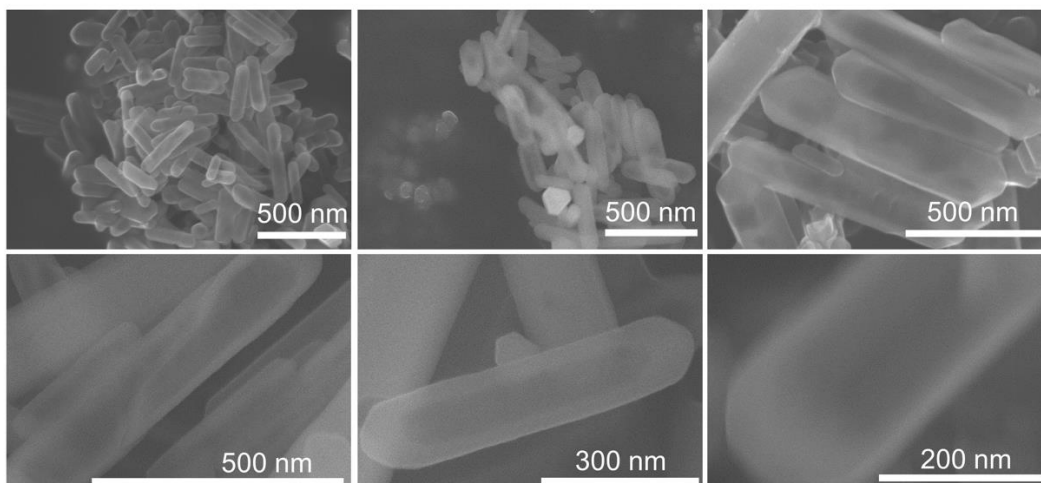


Figure S3. SEM images of capsular MOF.

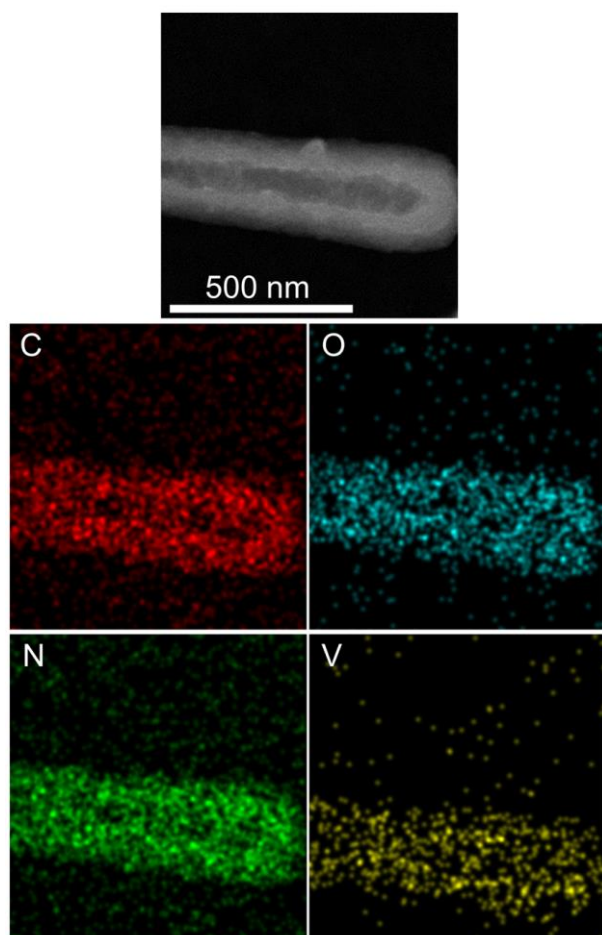


Figure S4. TEM image and the EDS mapping images of capsular MOF.

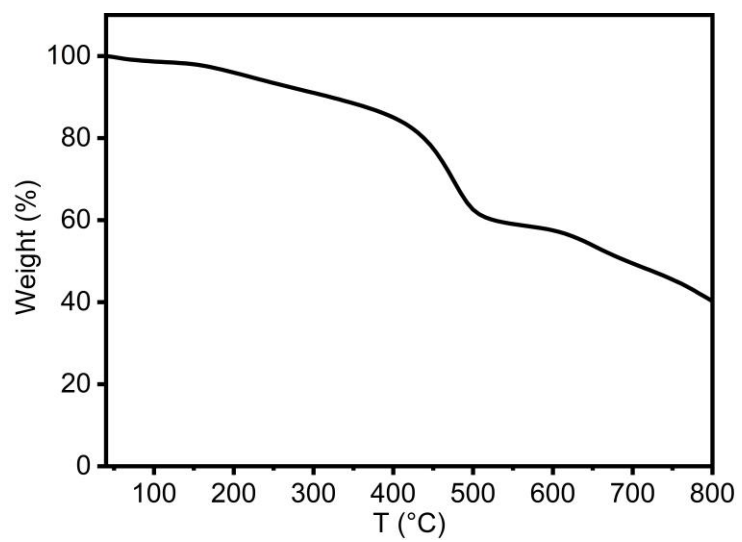
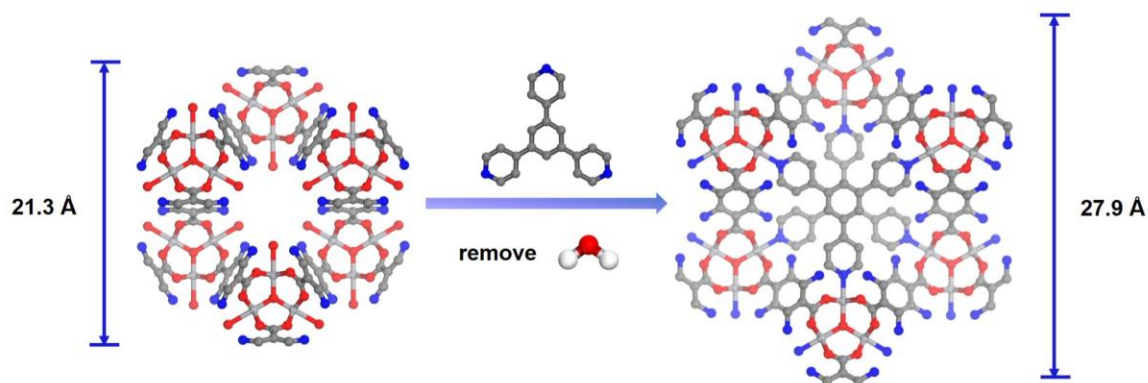


Figure S5. TGA curve of capsular MOF.



Compound	V-NH ₂ -MIL88B	V-NH ₂ -MIL88B-tpy
Crystal system	Hexagonal	Hexagonal
Space group	<i>P63/mmc</i>	<i>P63/mmc</i>
<i>a</i> , Å	12.9009	16.8853
<i>b</i> , Å	12.9009	16.8853
<i>c</i> , Å	18.2641	14.8612
α , deg	90	90
β , deg	90	90
γ , deg	120	120
<i>V</i> , Å ³	2632.50	3669.46

Figure S6. Predicted structural transformation mechanism and simulated cell parameters through DFT calculation. The dark gray, blue, red, white balls in represent C, N, O and V elements, respectively.

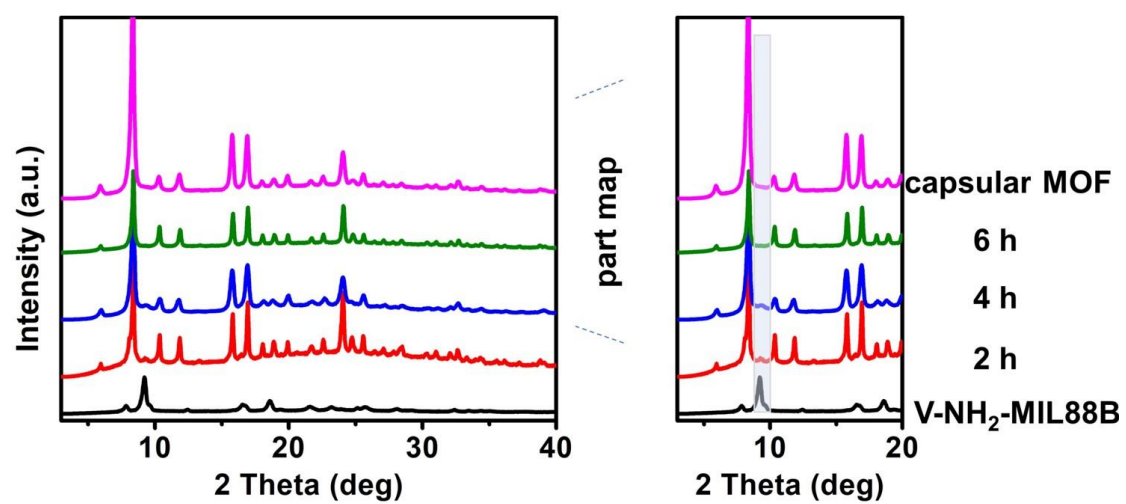


Figure S7. Time-dependent PXRD patterns of the intermediates for the synthesis of capsular MOF.

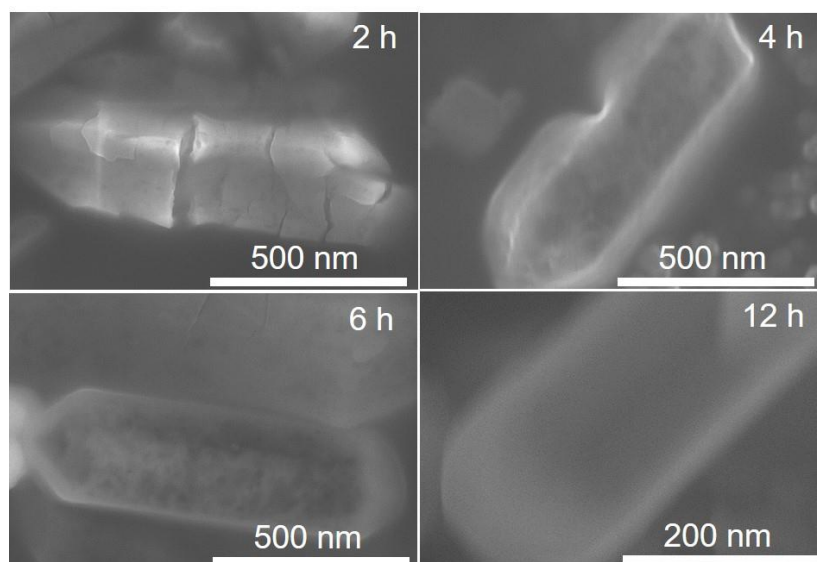


Figure S8. Time-dependent SEM images of intermediates in the synthetic process of capsular MOF.

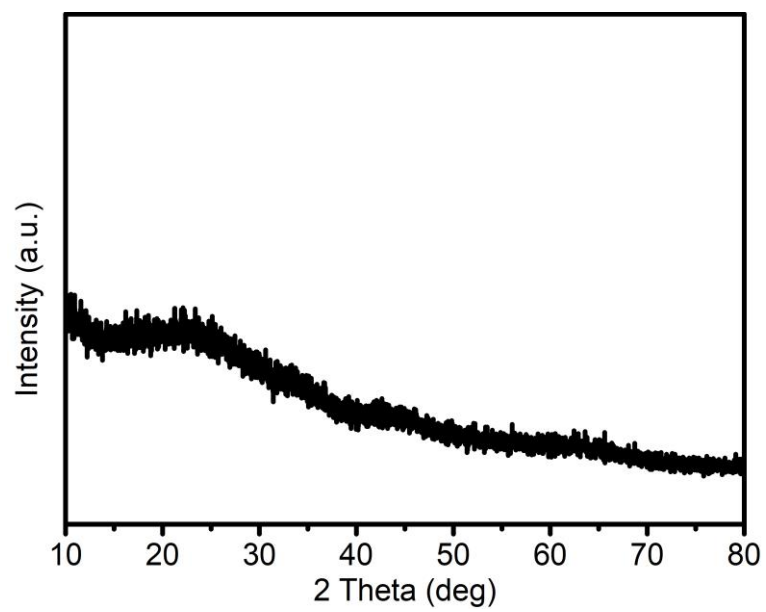


Figure S9. PXRD pattern of C-MOF-600.

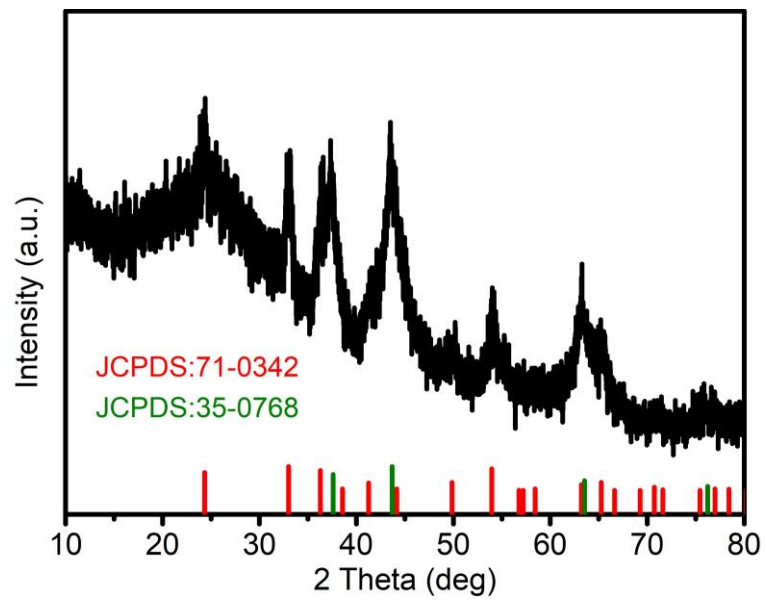


Figure S10. PXRD pattern of C-MOF-800.

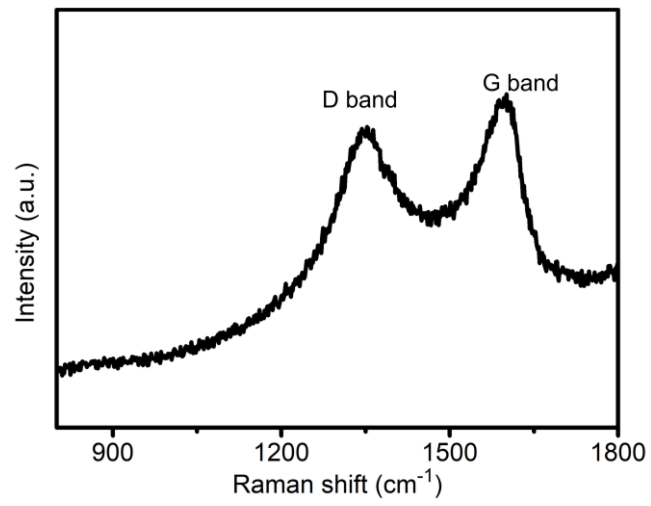


Figure S11. Raman spectrum of $V_xO_3@CN$.

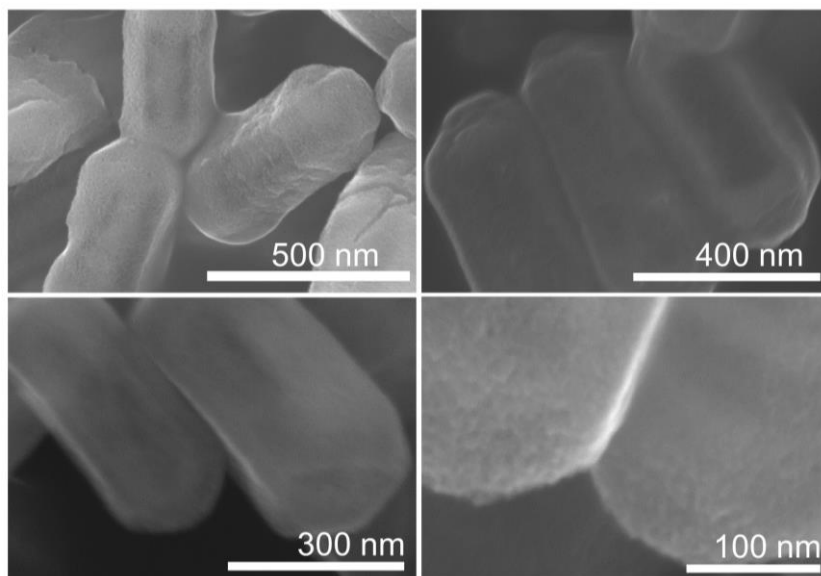


Figure S12. SEM images of $V_xO_3@CN$.

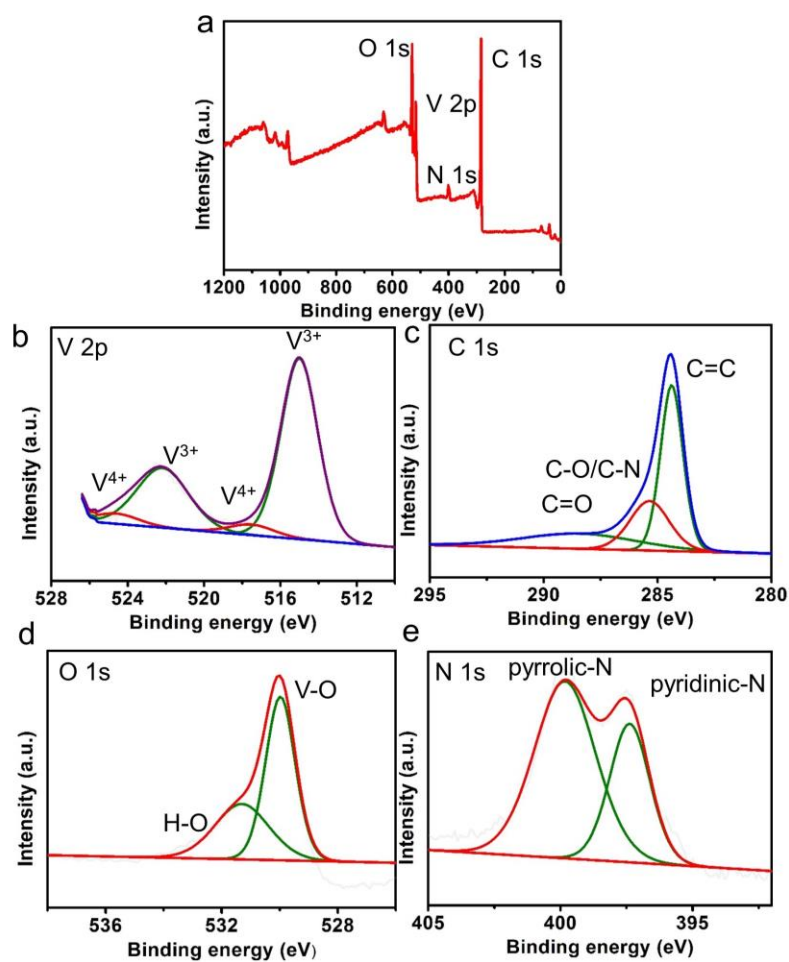


Figure S13. XPS of $V_xO_3@CN$. a) XPS survey of $V_xO_3@CN$, b) V 2p, c) C 1s, d) O 1s and e) N 1s of $V_xO_3@CN$.

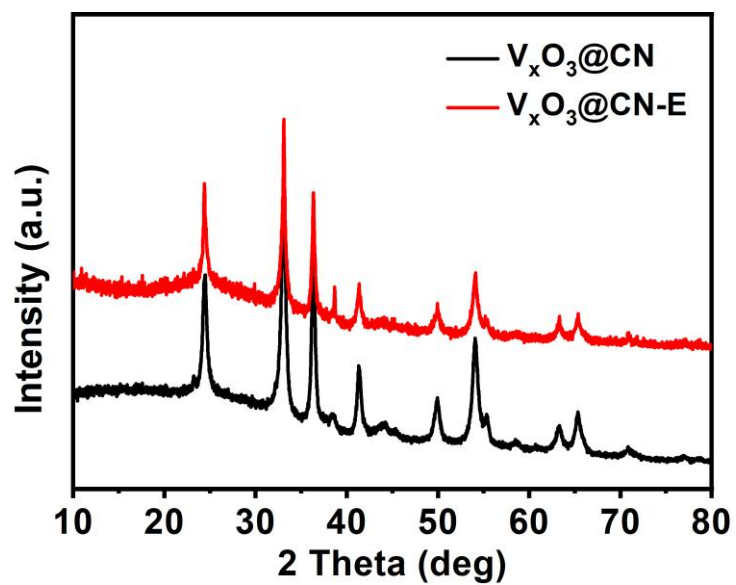


Figure S14. PXRD patterns of $V_xO_3@CN$ and $V_xO_3@CN$ after soaking into 3M $Zn(CF_3SO_3)_2$ electrolyte for seven days ($V_xO_3@CN-E$).

a



b



Figure S15. Contact angle images of a) V_2O_3 and b) $V_xO_3@CN$.

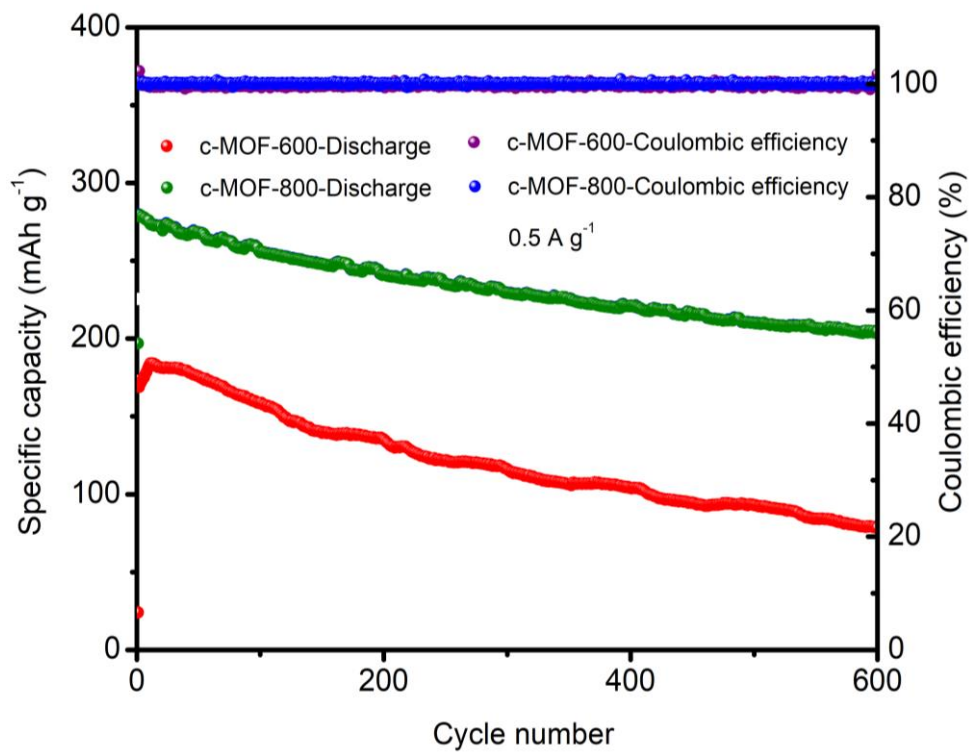


Figure S16. Cyclability of C-MOF-600 and C-MOF-800 electrode at 0.5 A g⁻¹.

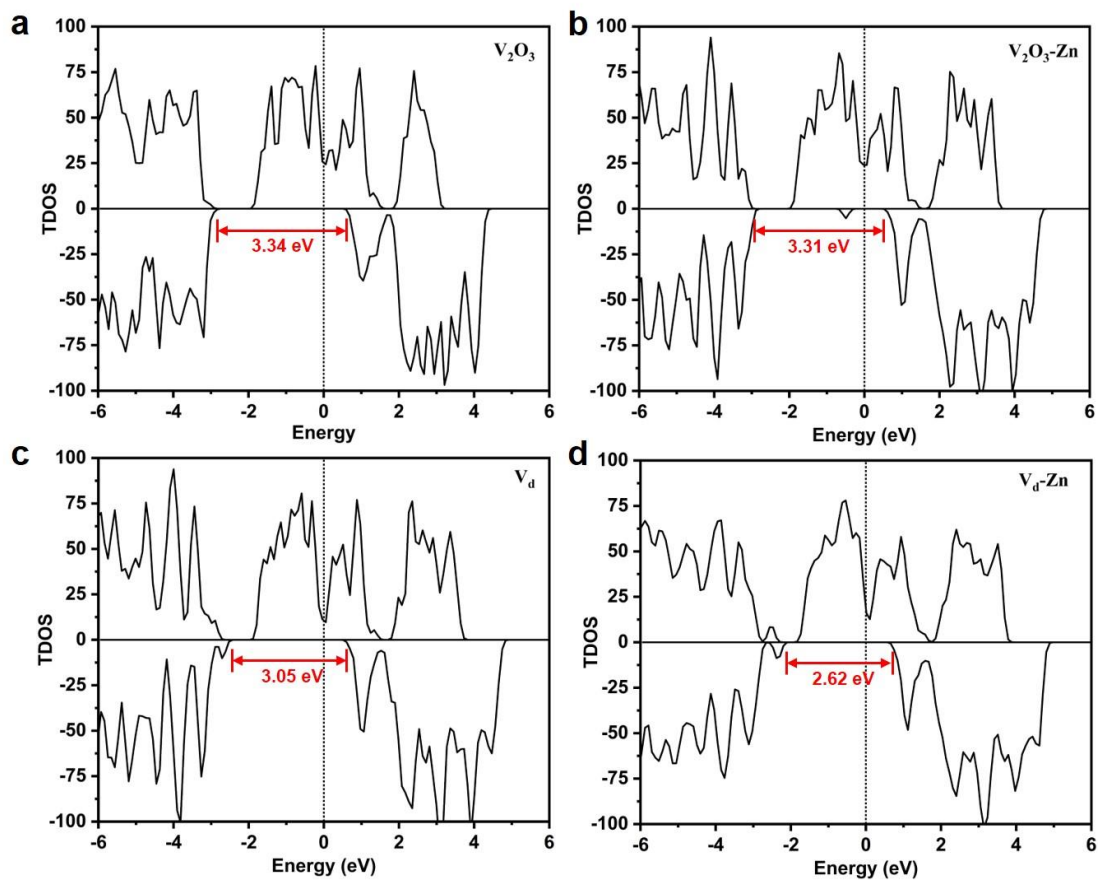


Figure S17. Calculated spin polarized projected total density of states (DOS) plots of a) V_2O_3 , b) V_2O_3 -Zn, c) V_d and d) V_d -Zn. (V_d = defective V_2O_3)

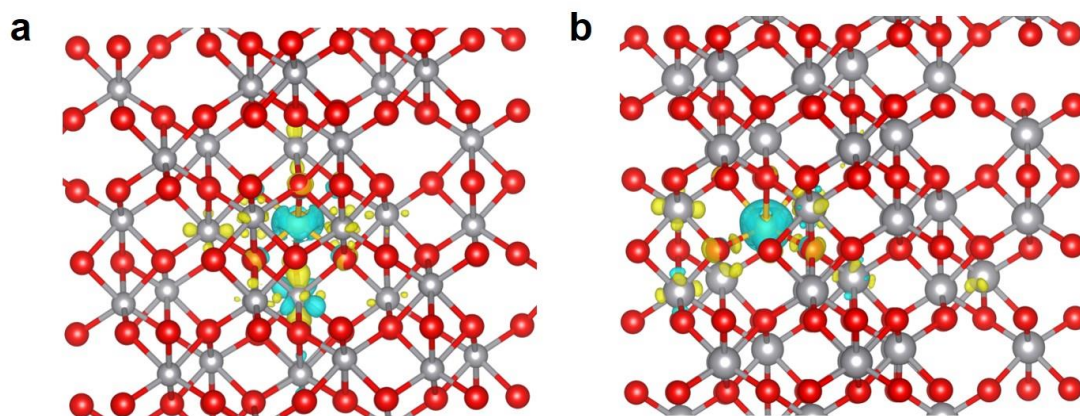


Figure S18. Charge density difference of a) V₂O₃-Zn and b) defective V₂O₃-Zn. The gray, red and gold balls in represent V, O and Zn elements, respectively.

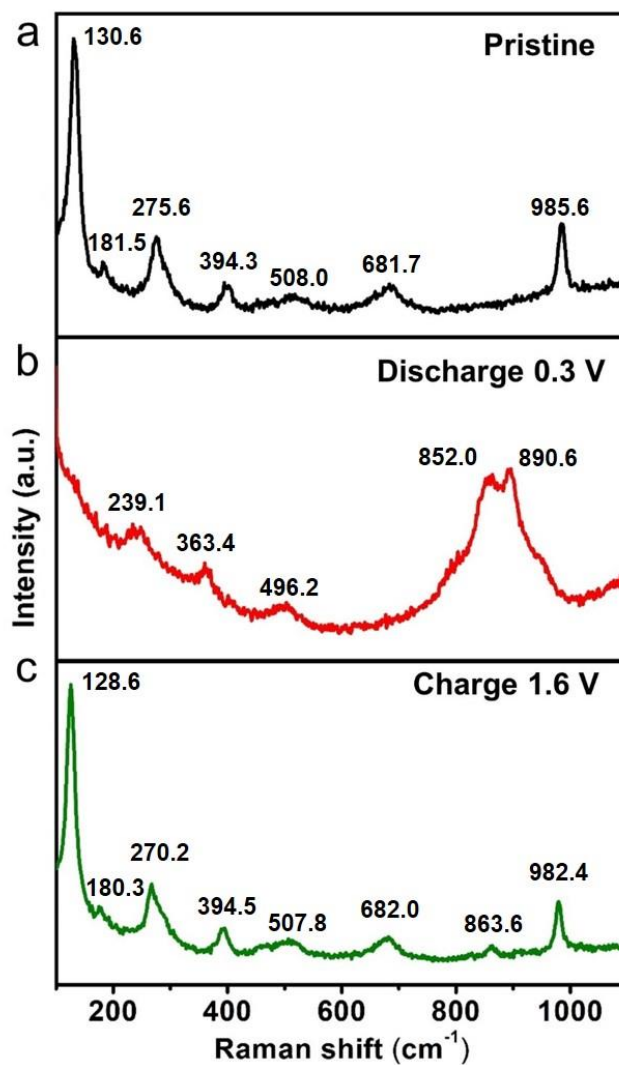


Figure S19. Raman spectra of $V_xO_3@CN$ electrode at fully charged and discharged states.

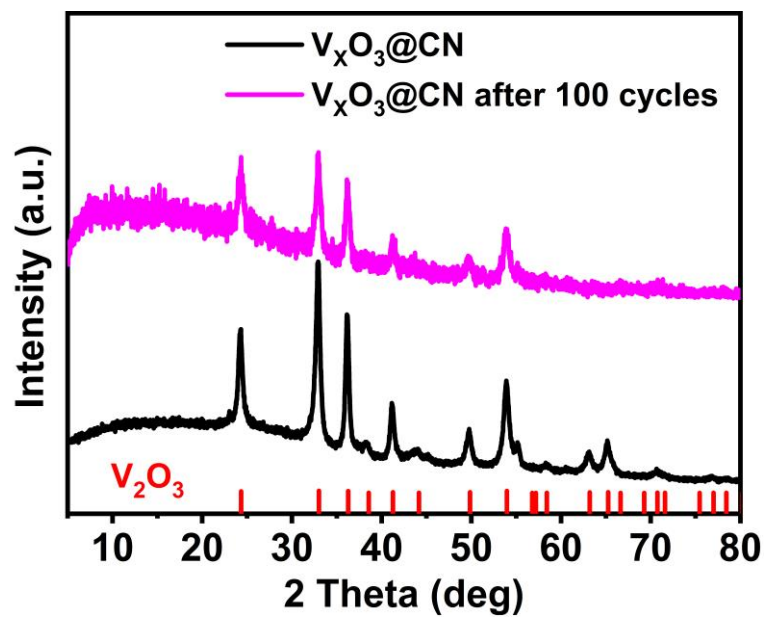


Figure S20. Post-cycle PXRD of $V_xO_3@CN$ electrode.

Table S1 Vanadium-based cathode for rechargeable aqueous zinc battery

Cathode material	Electrolyte	voltage (V)	Capacity (C/CD)	Cycling performance (C/CD/CN)	Ref.
$V_xO_3@CN$	3 M $Zn(CF_3SO_3)_2$	0.3-1.6	365/0.5	210/2/5000	This work
$V_2O_3@C$ NFs	2 M $Zn(CF_3SO_3)_2$	0.2-1.4	220/0.05	65/2/1000	[12]
V_2O_3	3 M $Zn(CF_3SO_3)_2$	0.2-1.6	383/0.4	225/3.2/800	[13]
$V_2O_3@SWCNH$ s@rGO	2 M $ZnSO_4$ + 2 M Na_2SO_4	0.2-1.6	422/0.2	283/5/1000	[14]
V_2O_3	2 M $Zn(CF_3SO_3)_2$	0.2-1.6	625/0.1	543/10/1000	[15]
$V_2O_3@C$	3 M $Zn(CF_3SO_3)_2$	0.3-1.5	350/0.1	170/5/4000	[16]
V_2O_3	3 M $Zn(CF_3SO_3)_2$	0.2-1.6	434/0.5	218/2/1000	[17]
V_2O_3	3 M $Zn(CF_3SO_3)_2$	0.1-1.3	196/0.1	100/5/30000	[18]
V-MOF derived porous V_2O_5 nanoplates	3 M $Zn(CF_3SO_3)_2$	0.3-1.5	240/0.1	120/2/2000	[19]
PEDOT- $NH_4V_3O_8$ PEDOT-NVO	3 M $Zn(CF_3SO_3)_2$	0.4-1.6	357/0.05	164/10/5000	[20]
$Na_{1.1}V_3O_{7.9}/rGO$	1 M $Zn(CF_3SO_3)_2$	0.76	238/0.05	140/1/1000	[21]
$Al_xV_2O_5$ -DMF	4 M $Zn(CF_3SO_3)_2$	0.2-1.8	407/0.1	240/5/2000	[22]
$VO_2 \cdot xH_2O$ Nanosheets	2 M $ZnSO_4$	0.2-1.6	337/0.2	159/10/1000	[23]

C: capacity (mAh g⁻¹), CD: current density (A g⁻¹), CN: cycle number

Table S2 Defect-engineered cathode materials for rechargeable aqueous zinc battery

Cathode material	Electrolyte	voltage (V)	Capacity (C/CD)	Cycling performance (C/CD/CN)	Ref.
$V_xO_3@CN$	3 M $Zn(CF_3SO_3)_2$	0.3-1.6	365/0.5	210/2/5000	This work
$Na_{0.76}V_6O_{15}/PE$ DOT	3 M $Zn(CF_3SO_3)_2$	0.3-1.5	355/0.05	244/10/1500	[24]
O-d- VO_2 -rG	3 M $Zn(CF_3SO_3)_2$	0.2-1.4	376/0.1	116/20/5000	[25]
V_6O_{13}	3 M $Zn(CF_3SO_3)_2$	0.2-1.5	410/0.2	283/5/1000	[26]
$VO_2 \cdot xH_2O$	2 M $ZnSO_4$	0.2-1.6	337/0.2	159/10/1000	[27]
$NH_4V_4O_{10}$	3 M $Zn(CF_3SO_3)_2$	0.3-1.7	435/0.2	244/10/1500	[28]
PEDOT- $NH_4V_3O_8$	3 M $Zn(CF_3SO_3)_2$	0.4-1.6	356.8/0.05	163.6/10/1000	[29]
Vö- V_2O_5 - PEDOT	3 M $Zn(CF_3SO_3)_2$	0.3-1.6	449/0.2	318/10/6000	[30]
β - MnO_2	3 M $ZnSO_4+0.1$ M $MnSO_4$	0.8-1.8	302/0.05	200/0.5/300	[31]
$Al_{0.35}Mn_{2.52}O_4$	2.5 M $ZnSO_4+0.2$ M $MnSO_4$	0.95- 1.85	302/0.1	147/1.5/1000	[32]
CaVO	2 M $ZnSO_4$	0.9-1.85	310/0.5	310/0.5/3000	[33]
$MnCo_2O_4$	2.0 M $ZnSO_4+0.5$ M $MnSO_4$	0.8-1.8	660/0.05	70/0.2/800	[34]

C: capacity (mAh g⁻¹), CD: current density (A g⁻¹), CN: cycle number

References

- 1 K.-J. Chen, J. John, S. Scott, Q.-Y. Yang, M. J. Zaworotko, *Chem. Sci.* 2015, **6**, 4784-4789.
- 2 I. E. Rauda, V. Augustyn, B. Dunn, S. H. Tolbert, *Acc. Chem. Res.* 2013, **46**, 1113-1124.
- 3 Z. Shen, L. Cao, C. D. Rahn, C.-Y. Wang, *J. Electrochem. Soc.* 2013, **160**, A1842.
- 4 J. P. Perdew, K. Burke, M. Ernzerhof, *Phys. Rev. Lett.* 1996, **77**, 3865-3868.
- 5 G. Kresse, J. Furthmüller, *Comp. Mater. Sci.* 1996, **6**, 15-50.
- 6 G. Kresse, J. Hafner, *Phys. Rev. B* 1993, **47**, 558-561.
- 7 G. Kresse, J. Hafner, *Phys. Rev. B* 1994, **49**, 14251-14269.
- 8 G. Kresse, J. Furthmüller, *Phys. Rev. B* 1996, **54**, 11169-11186.
- 9 J. Goniakowski, C. Noguera, *J. Phys. Chem. C* 2019, **123**, 9272-9281.
- 10 H. J. Monkhorst, J. D. Pack, *Phys. Rev. B* 1976, **13**, 5188-5192.
- 11 G. Henkelman, B. P. Uberuaga, H. Jónsson, *J. Chem. Phys.* 2000, **113**, 9901-9904.
- 12 X. Liu, Z. Wang, Y. Niu, C. Liu, H. Chen, X. Ren, Z. Liu, W.-M. Lau, D. Zhou, *ACS Appl. Energy Mater.* 2022, **5**, 3525-3535.
- 13 J. Ding, H. Zheng, H. Gao, Q. Liu, Z. Hu, L. Han, S. Wang, S. Wu, S. Fang, S. Chou, *Adv. Energy Mater.* 2021, **11**, 2100973.
- 14 J. Hong, L. Xie, C. Shi, X. Lu, X. Shi, J. Cai, Y. Wu, L. Shao, Z. Sun, *Small Methods* 2024, **8**, 2300205.
- 15 H. Luo, B. Wang, F. Wang, J. Yang, F. Wu, Y. Ning, Y. Zhou, D. Wang, H. Liu, S. Dou, *ACS Nano* 2020, **14**, 7328-7337.
- 16 Y. Ding, Y. Peng, S. Chen, X. Zhang, Z. Li, L. Zhu, L.-E. Mo, L. Hu, *ACS Appl. Mater. Inter.* 2019, **11**, 44109-44117.
- 17 K. Hu, D. Jin, Y. Zhang, L. Ke, H. Shang, Y. Yan, H. Lin, K. Rui, J. Zhu, *J. Energy Chem.* 2021, **61**, 594-601.
- 18 K. Zhu, S. Wei, H. Shou, F. Shen, S. Chen, P. Zhang, C. Wang, Y. Cao, X. Guo, M. Luo, H. Zhang, B. Ye, X. Wu, L. He, L. Song, *Nat. Commun.* 2021, **12**, 6878.
- 19 Y. Ding, Y. Peng, W. Chen, Y. Niu, S. Wu, X. Zhang, L. Hu, *Appl. Surf. Sci.* 2019, **493**, 368-374.
- 20 H. Y. Shi, X. Sun, *Chem* 2020, **6**, 817-819.
- 21 Y. Wang, L. Zhou, X. Cao, X. Gao, X. Lu, *J. Mater. Chem. A* 2021, **9**, 26698-26703.

- 22 F. Wan, Z. Hao, S. Wang, Y. Ni, J. Zhu, Z. Tie, S. Bi, Z. Niu, J. Chen. *Adv. Mater.* 2021, **33**, 2102701.
- 23 Y. Wang, L. Zhou, X. Cao, X. Gao, X. Lu, *J. Mater. Chem. A* 2021, **9**, 26698-26703.
- 24 W. Bi, G. Gao, G. Wu, M. Atif, M. AlSalhi, G. Cao, *Energy Storage Mater.* 2021, **40**, 209.
- 25 H. Luo, B. Wang, C. Wang, F. Wu, F. Jin, B. Cong, Y. Ning, Y. Zhou, D. Wang, H. Liu, *Energy Storage Mater.* 2020, **33**, 390.
- 26 M. Liao, J. Wang, L. Ye, H. Sun, Y. Wen, C. Wang, X. Sun, B. Wang, H. Peng, *Angew. Chem. Int. Ed.* 2020, **59**, 2273.
- 27 Z. Zhang, B. Xi, X. Wang, X. Ma, W. Chen, J. Feng, S. Xiong, *Adv. Funct. Mater.* 2021, **31**, 2103070.
- 28 J. Li, N. Luo, F. Wan, S. Zhao, Z. Li, W. Li, J. Guo, P. R. Shearing, D. J. Brett, C. J. Carmalt, *Nanoscale* 2020, **12**, 20638.
- 29 D. Bin, W. Huo, Y. Yuan, J. Huang, Y. Liu, Y. Zhang, F. Dong, Y. Wang, Y. Xia, *Chem* 2020, **6**, 968.
- 30 Y. Du, X. Wang, J. Sun, *Nano Res.* 2021, **14**, 754.
- 31 M. Han, J. Huang, S. Liang, L. Shan, X. Xie, Z. Yi, Y. Wang, S. Guo, J. Zhou, *iScience* 2020, **23**, 100797.
- 32 D. Wang, S. Zhang, C. Li, X. Chen, W. Zhang, X. Ge, H. Lin, Z. Shi, S. Feng, *Small* 2022, **18**, 2105970.
- 33 J. Gao, C. Cheng, L. Ding, G. Liu, T. Yan, L. Zhang, *Chem. Eng. J* 2022, **450**, 138367.
- 34 N. Yadav, J. Qin, T. Maiyalagan, W. Limphirat, A. Khampuanbut, P. Pattananuwat, *Electrochim. Acta* 2024, **500**, 144776.